



*Supplement of*

**Evaluation of global EMEP MSC-W (rv4.34) WRF (v3.9.1.1) model surface concentrations and wet deposition of reactive N and S with measurements**

**Yao Ge et al.**

*Correspondence to:* Yao Ge ([y.ge-7@sms.ed.ac.uk](mailto:y.ge-7@sms.ed.ac.uk)) and Mathew R. Heal ([m.heal@ed.ac.uk](mailto:m.heal@ed.ac.uk))

The copyright of individual parts of the supplement might differ from the article licence.

## Table of Contents

	Model evaluation statistics (Text).....	2
	NO <sub>x</sub> and SO <sub>x</sub> emission differences between HTAP and ECLIPSE <sub>E</sub> inventories (Fig. S1 and S2) .....	3
5	Comparisons of monthly profiles of the HTAP and ECLIPSE <sub>E</sub> emission inventories (Text, Fig. S3 and S4).....	4
	Comparisons between use of HTAP and ECLIPSE <sub>E</sub> emission inventories: NH <sub>4</sub> <sup>+</sup> concentration (Text and Fig. S5).....	6
	Evaluation of model response to changes between 2010 and 2015 ECLIPSE <sub>E</sub> emissions (Text, Fig. S6-S9 and Table S1).....	8
	Comparison of temporal variation of modelled NH <sub>4</sub> <sup>+</sup> concentrations with measurements (Fig. S10).....	17
	Comparison of modelled precipitation and wet deposition with measurements (Fig. S11 and Table S2) .....	18

10

## Model evaluation statistics

- 15 The unit of atmospheric concentration used in this work is  $\mu\text{g m}^{-3}$ . The ppb mixing ratios of gaseous species downloaded from some network websites were converted to mass concentrations via the ideal gas law ( $pV = nRT$ ) and assuming 1 atmosphere pressure:

$$\mu\text{g m}^{-3} = \frac{\text{ppb} \times M}{0.0821 \times (273.15 + T)}$$

- 20 where  $T$  is the temperature in  $^{\circ}\text{C}$ ,  $M$  is molecular mass of the gaseous pollutant ( $\text{g mol}^{-1}$ ) and  $0.0821 \text{ L atm K}^{-1} \text{ mol}^{-1}$  is the ideal gas constant  $R$ .

The following statistical metrics were calculated to compare model and observation data where  $M_i$  and  $O_i$  are modelled and observed (i.e. measured) data in a dataset of  $n$  such pairs. If a model grid contains more than one measurement site, the average of the measurements is used as  $O_i$ .

Pearson's correlation coefficient:

25

$$R = \frac{\sum_{i=1}^n (M_i - \bar{M})(O_i - \bar{O})}{\sqrt{\sum_{i=1}^n (M_i - \bar{M})^2} \sqrt{\sum_{i=1}^n (O_i - \bar{O})^2}}$$

Mean bias:

$$M_B = \frac{1}{n} \sum_{i=1}^n (M_i - O_i) = \bar{M} - \bar{O}$$

Mean absolute error:

$$M_E = \frac{1}{n} \sum_{i=1}^n |M_i - O_i|$$

- 30 Normalized mean bias:

$$NMB = \frac{\sum_{i=1}^n (M_i - O_i)}{\sum_{i=1}^n O_i} = \left( \frac{\bar{M}}{\bar{O}} - 1 \right)$$

Normalized mean error:

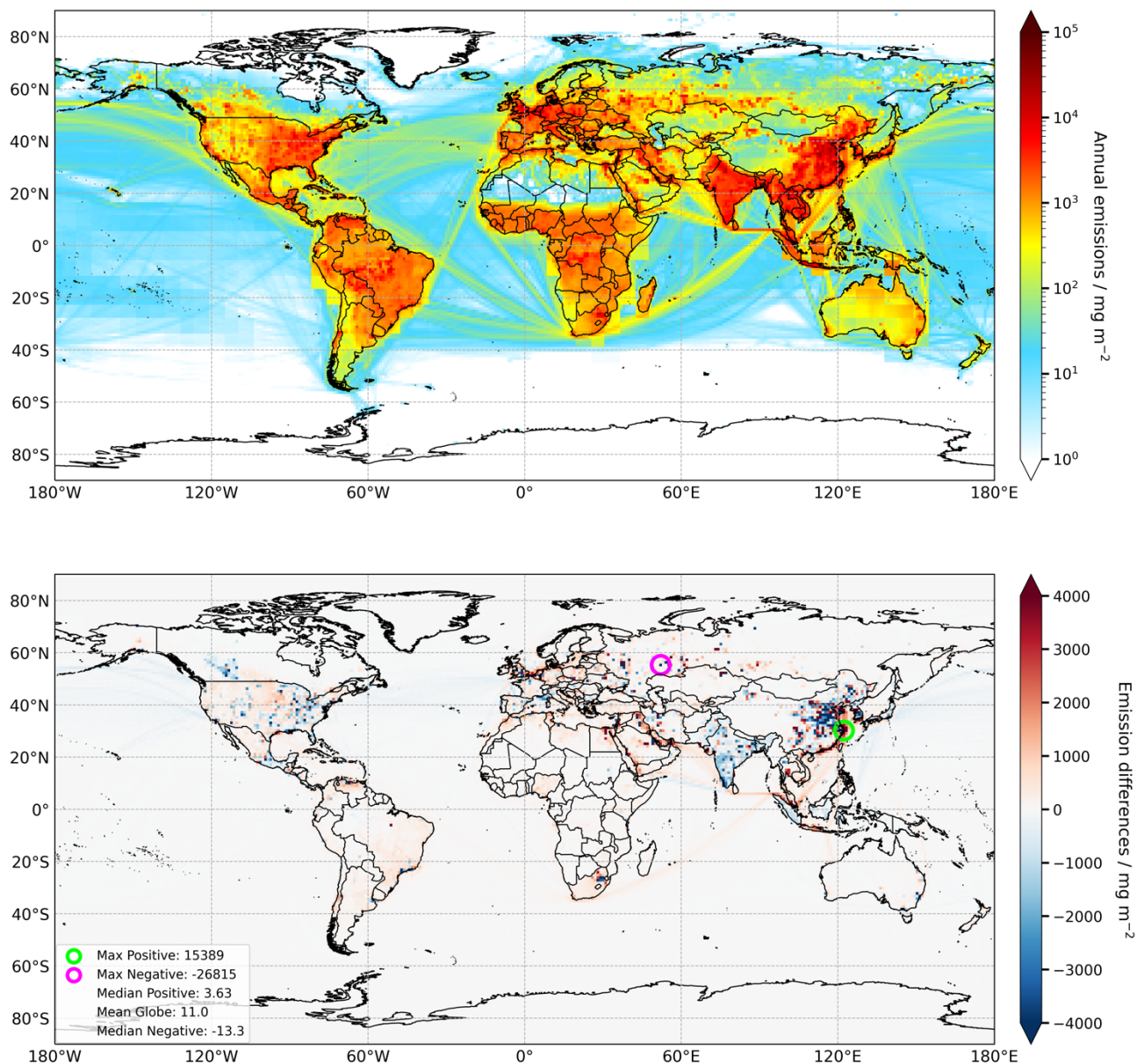
$$NME = \frac{\sum_{i=1}^n |M_i - O_i|}{\sum_{i=1}^n O_i} = \frac{M_E}{\bar{O}}$$

35

40

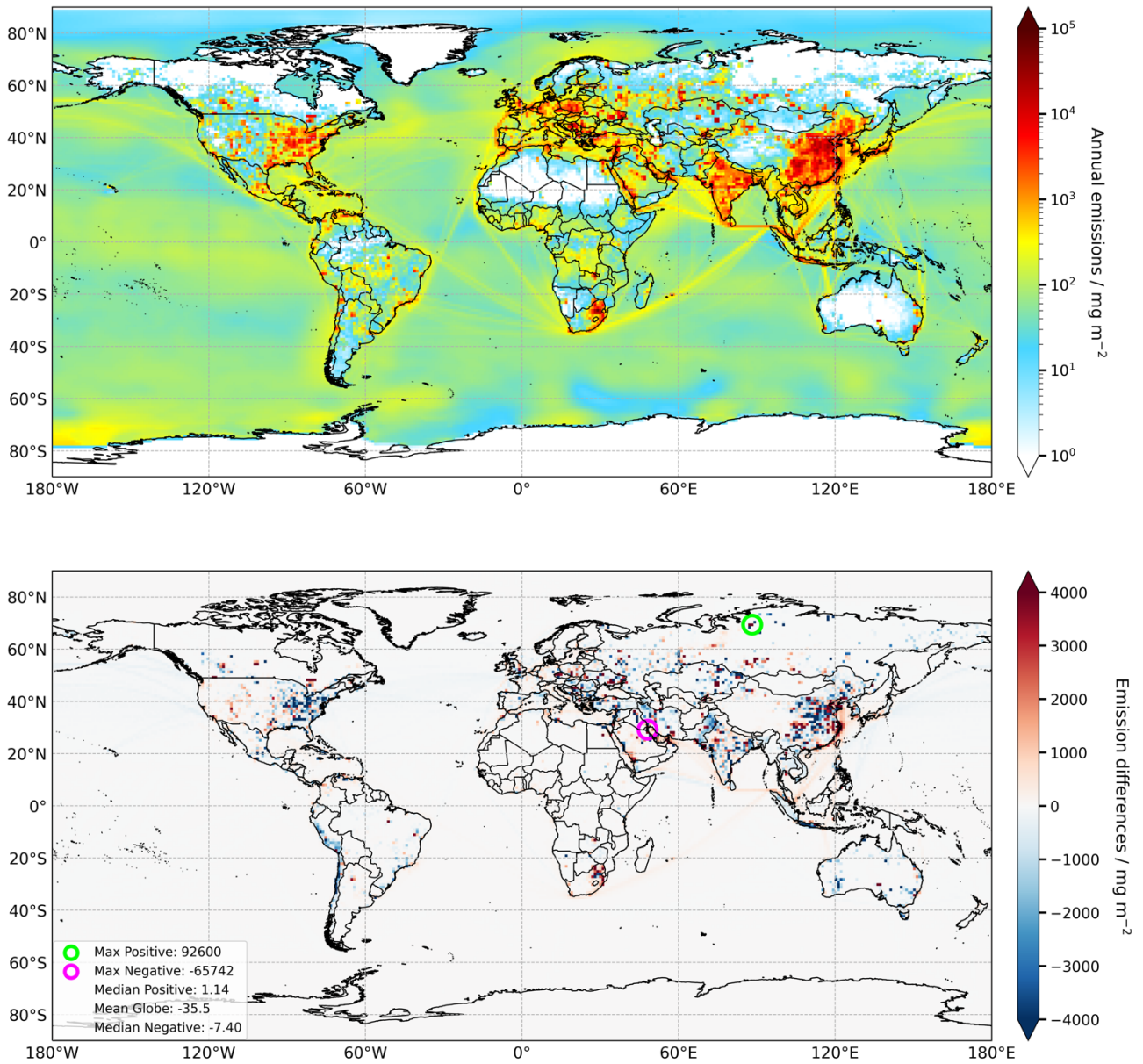
45

## NO<sub>x</sub> and SO<sub>x</sub> emission differences between HTAP and ECLIPSE<sub>E</sub> inventories



50

Figure S1. Top: Global annual NO<sub>x</sub> emissions for 2010 from ECLIPSE<sub>E</sub>. Bottom: the difference in 2010 annual NO<sub>x</sub> emissions (mg m<sup>-2</sup>) between ECLIPSE<sub>E</sub> and HTAP (ECLIPSE<sub>E</sub> – HTAP). The inset panel provides the maximum, median and mean values of both positive and negative differences across individual emission grids.



55

**Figure S2. Top: Global annual SO<sub>x</sub> emissions for 2010 from ECLIPSE<sub>E</sub>. Bottom: the difference in 2010 annual SO<sub>x</sub> emissions (mg m<sup>-2</sup>) between ECLIPSE<sub>E</sub> and HTAP (ECLIPSE<sub>E</sub> – HTAP). The inset panel provides the maximum, median and mean values of both positive and negative differences across individual emission grids.**

60

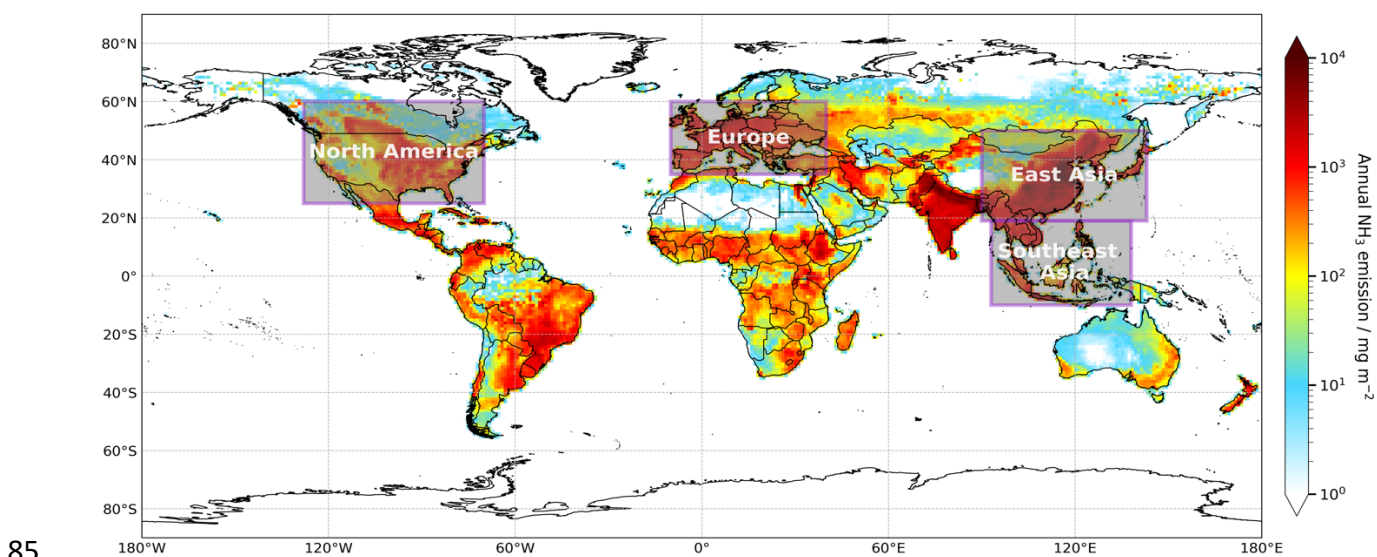
### Comparisons of monthly profiles of the HTAP and ECLIPSE<sub>E</sub> emission inventories

Figure S3 presents a global map of annual terrestrial NH<sub>3</sub> emissions from ECLIPSE<sub>E</sub> (i.e. ECLIPSE annual total emission with EDGAR monthly profile) in 2010. The boxes on the map delineate four example regions with measurement networks that are subsequently used to compare model and measurement concentrations spatially and seasonally, as reported in the main paper. Figure S4 compares the spatially-averaged monthly NH<sub>3</sub> emissions of the HTAP and ECLIPSE<sub>E</sub> inventories in 2010 in each of these four global regions.

65

70 There is clear seasonality in NH<sub>3</sub> emissions in all four regions. In East Asia, the ECLIPSE<sub>E</sub> inventory has larger NH<sub>3</sub> emissions than the HTAP inventory across all months and has a prominent maximum in spring, in addition to the general elevated emissions in summer projected by both inventories. For Southeast Asia, both the HTAP and ECLIPSE<sub>E</sub> inventories present a distinct peak in NH<sub>3</sub> emissions in March, with the HTAP inventory having larger emissions than the ECLIPSE<sub>E</sub> inventory in most months of the year, particularly in winter (as a consequence of smaller annual variation in the HTAP NH<sub>3</sub> emissions).

75 In Europe and North America there is generally good coincidence in magnitude and seasonality of NH<sub>3</sub> emissions between the two inventories. In Europe, both inventories project maximum NH<sub>3</sub> emissions in March and April, although the ECLIPSE<sub>E</sub> inventory also projects a second maximum in August. The annual average emissions in Europe are similar, with sometimes one inventory and sometimes the other having higher emission in an individual month. In contrast, in North America, both inventories project maximum NH<sub>3</sub> emissions in July and August and much less pronounced peaks in early spring. In this region it is the HTAP inventory that projects the greatest annual variation, in contrast to East and Southeast Asia where ECLIPSE<sub>E</sub> projects the greatest annual variation. The spring and summer peaks in NH<sub>3</sub> emissions in all four world regions reflect both agricultural activities (the dominant source of NH<sub>3</sub>) and meteorological conditions. Larger NH<sub>3</sub> emissions in spring are associated with intensive manure and synthetic fertilizer application, whilst the rising temperatures throughout the summer favour the volatilisation of NH<sub>3</sub> from all sources.



80 **Figure S3. Global annual NH<sub>3</sub> emissions (mg m<sup>-2</sup>) for 2010 from the ECLIPSE<sub>E</sub> inventory as implemented in the EMEP MSC-W model simulations in this work. The grey boxes show four regions in which monthly emission profiles of the ECLIPSE<sub>E</sub> and HTAP inventories are compared.**

90

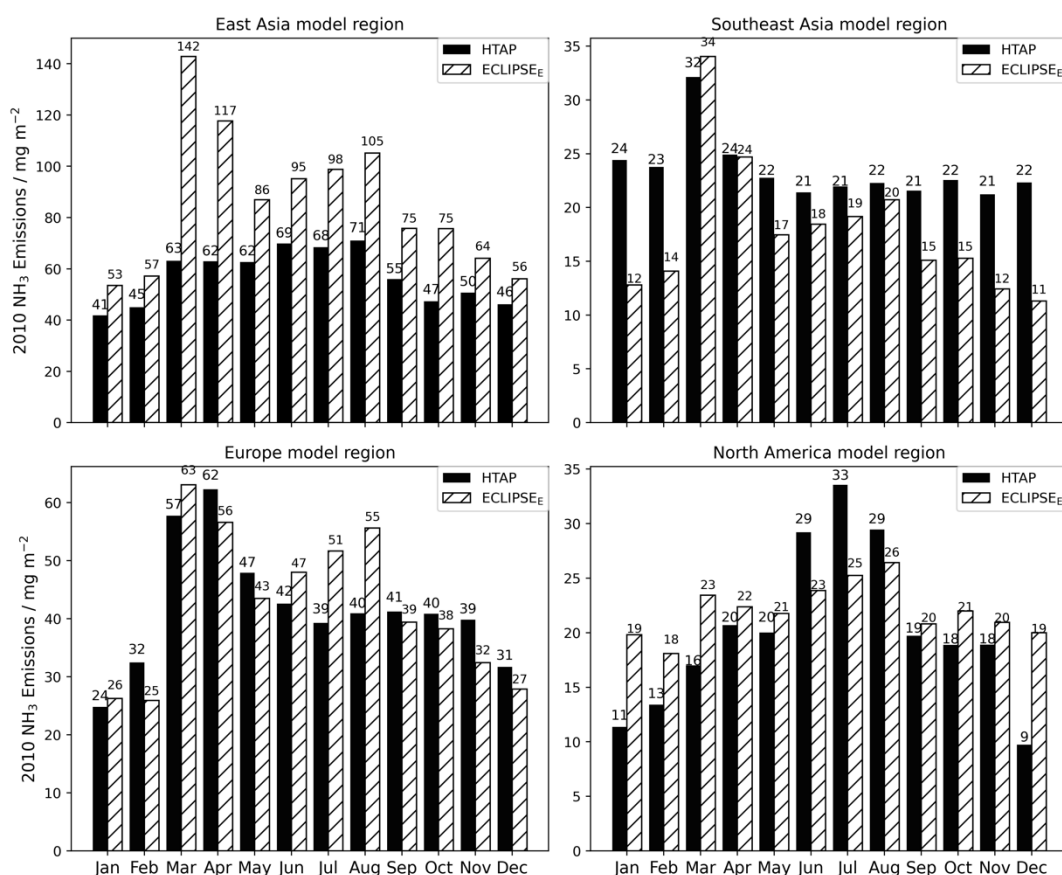


**Figure S4. Monthly variations in the 2010 NH<sub>3</sub> emissions per unit area of the HTAP and ECLIPSE<sub>E</sub> inventories averaged across each of the four model regions illustrated in Fig. S3: East Asia, Southeast Asia, Europe and North America. Note the different vertical scales in each panel.**

95

### Comparisons between use of HTAP and ECLIPSE<sub>E</sub> emission inventories: NH<sub>4</sub><sup>+</sup> concentration

The influences of the two emission inventories on model simulated surface concentration differs according to consideration of primary or secondary component and varies from one region to another. In general, concentrations of primary pollutants are more influenced by the local emissions, while secondary species are much less so. Fig. S5 compares the modelled NH<sub>4</sub><sup>+</sup> concentrations using the two emission inventories for the grids in which there are also available measurements from the monitoring networks.

100

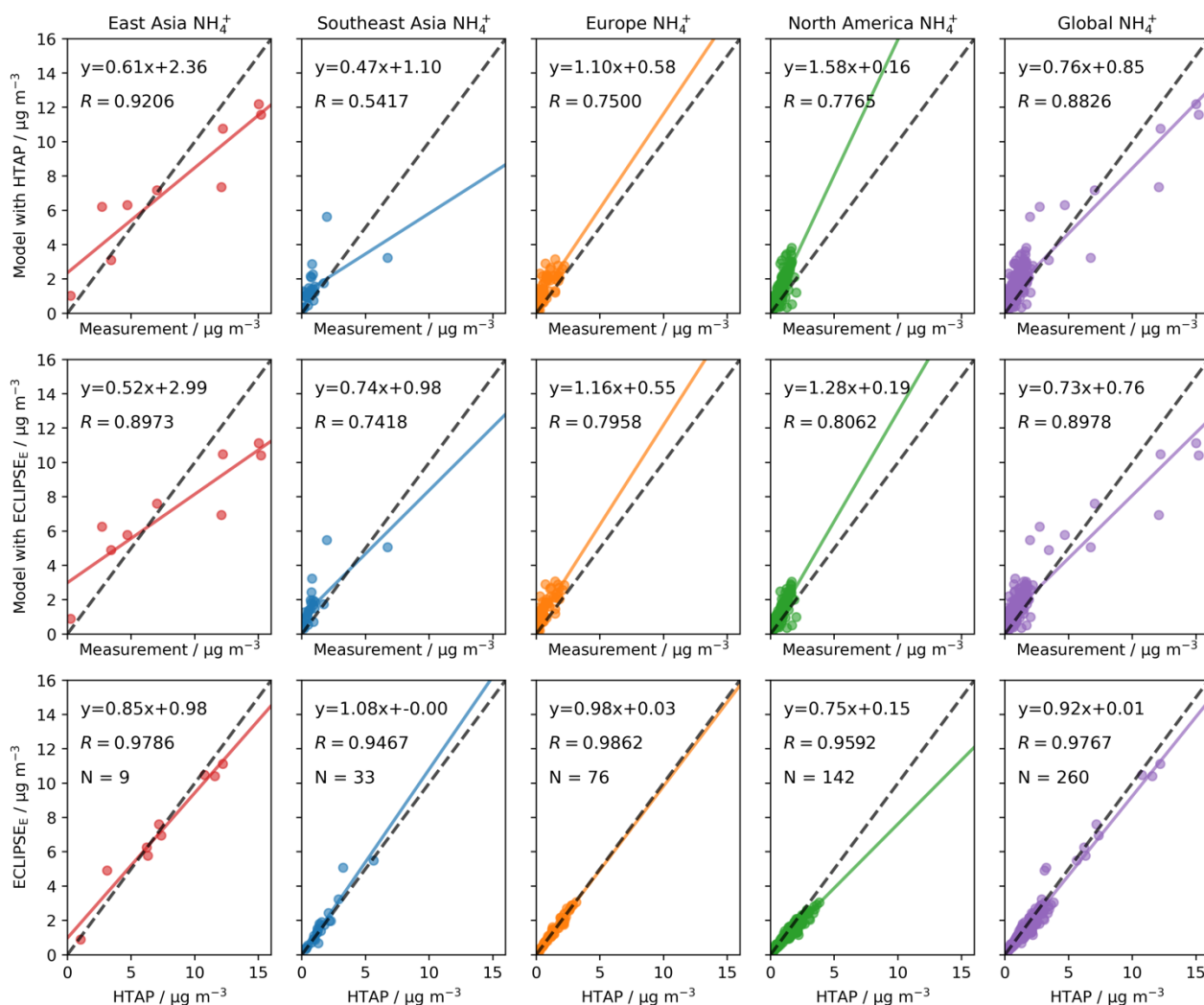
The differences in NH<sub>4</sub><sup>+</sup> concentrations in simulations using the two emission inventories are smaller than for NH<sub>3</sub> (Fig. 4), as shown by concentrations that are closer to 1:1 in all regions. For example, whilst modelled NH<sub>3</sub> concentrations in China derived using the ECLIPSE<sub>E</sub> inventory are on average 56% higher than those derived using the HTAP inventory, the NH<sub>4</sub><sup>+</sup> concentrations are very similar. The annual average NH<sub>4</sub><sup>+</sup> concentrations (based on network locations) in China are 7.30 and 7.15 μg m<sup>-3</sup> for HTAP and ECLIPSE<sub>E</sub> respectively, which is a difference of only 2%. The regression equation of NH<sub>4</sub><sup>+</sup> concentrations from the model simulations with the two inventories across the full set of measurement network locations considered in this work is excellent ( $y = 0.92x + 0.01$ ,  $R = 0.98$ , Fig. S5). This indicates good global consistency for the WRF-EMEP modelling system across a wide variation of primary NH<sub>3</sub>, NO<sub>2</sub> and SO<sub>2</sub> emissions in different global regions. It can be noted, however, that model simulations with both HTAP and ECLIPSE<sub>E</sub> inventories yield slightly higher

105

110

concentrations than measurements at lower concentrations (below  $5 \mu\text{g m}^{-3}$ ) but lower concentrations than measurements at higher concentration ranges. This reflects a fundamental difference between modelled and measured data. The modelled value represents the average concentration over a grid of several 10s km in horizontal dimension, whereas the measured values only represent the concentration at the specific location of the measurement. Since the latter are readily impacted by local sources and sinks, they will generally have a greater range in values which are averaged out in the former. Measurements are also sometimes deliberately sited in locations of anticipated high pollutant concentration that may be reduced by grid averaging in relatively spatially coarse global model simulations.

115



120

**Figure S5. Comparisons of annual average surface concentrations of NH<sub>4</sub><sup>+</sup> for 8 monitoring networks in 2010 – NNDMN from China as East Asia, EANET as Southeast Asia, NAMN and AGANet (UK) and EMEP/CCC plotted together here as Europe, and the EPA and AMoN (USA) and NAPS (Canada) plotted together here as North America – and for all networks combined ('global'). The upper row of plots is modelled versus measured using the HTAP emission inventory. The middle row is modelled versus measured using the ECLIPSE<sub>E</sub> emission inventory. The lower row is the modelled data for the two inventories plotted against each other for the same set of model grids that contain measurement sites. In each plot, N is the total number of scatter points, R is the Pearson correlation coefficient, the black dashed line is the 1:1 line and the coloured solid line is the trend line corresponding to the equation presented.**

125

130

## Evaluation of model response to changes between 2010 and 2015 ECLIPSE<sub>E</sub> emissions

This section describes modelled concentration and deposition responses to the changes in emissions for the two simulations for 2010 and 2015 that use ECLIPSE<sub>E</sub> emissions data.

135 Figure S6 first shows how the spatial distributions in annual NH<sub>3</sub>, NO<sub>x</sub>, and SO<sub>x</sub> emissions changed between the 2010 and 2015 ECLIPSE<sub>E</sub> inventories. Emissions of NH<sub>3</sub> increased from 2010 to 2015 in China, India, Southeast Asian countries, Germany, Italy, Central African countries, United States and Mexico, while NH<sub>3</sub> emissions both increased and decreased in some South African countries, Latin American countries, Russia, and Canada. Overall, however, emission changes of NH<sub>3</sub> between 2010 and 2015 are generally small: 73% of the relative differences are within ± 15% of 2010 ECLIPSE<sub>E</sub> inventory emission for that grid. The global average trend in NH<sub>3</sub> emissions is slightly upward, with a global area-weighted average increase of 5.46 mg m<sup>-2</sup> (= 4.5%) in the 2015 ECLIPSE<sub>E</sub> inventory compared with the 2010 inventory. In contrast, NO<sub>x</sub> and SO<sub>x</sub> emissions show slightly different patterns. Both NO<sub>x</sub> and SO<sub>x</sub> emissions declined strongly in eastern China, Europe, and United States between 2010 and 2015, whereas they increased in India. Across all model grids, 58% and 52% of relative differences in NO<sub>x</sub> and SO<sub>x</sub> ECLIPSE<sub>E</sub> inventory emissions in 2015 are within ± 15% of their 2010 values respectively. Worldwide, the emissions of both these precursors decreased from 2010 to 2015: the global area-weighted average differences of NO<sub>x</sub> and SO<sub>x</sub> emissions are -22.1 mg m<sup>-2</sup> and -31.3 mg m<sup>-2</sup>, which equate to -5.7% and -14% of their average emissions for 2010 respectively.

145 Figures S7 and S8 respectively show the changes in the modelled atmospheric concentrations of the gases NH<sub>3</sub>, NO<sub>2</sub>, and SO<sub>2</sub>, and the secondary aerosol species NH<sub>4</sub><sup>+</sup>, NO<sub>3</sub><sup>-</sup>, and SO<sub>4</sub><sup>2-</sup>, between 2010 and 2015. Most parts of the world show increased NH<sub>3</sub> concentrations but decreased NO<sub>2</sub> and SO<sub>2</sub> concentrations from 2010 to 2015 (Figure S7). In general, the NH<sub>3</sub>, NO<sub>2</sub>, and SO<sub>2</sub> annual concentration changes are consistent with their corresponding emission changes in spite of potential differential meteorological influences on concentrations between the two years, which indicates the modelling system is capable of capturing the influence of emission changes on atmospheric concentrations. Variations in SO<sub>4</sub><sup>2-</sup> concentrations are similar to those for NH<sub>4</sub><sup>+</sup> but show opposite trends in comparison to NO<sub>3</sub><sup>-</sup> especially in India and eastern China regions (Figure S8), due to the preferential reaction between NH<sub>3</sub> and H<sub>2</sub>SO<sub>4</sub>, and the stability of ammonium sulphate. The impact of emission variations on concentrations of secondary pollutants is less clear than for primary pollutants since the former are influenced by multiple emissions and meteorological factors, and because the timescales (and hence spatial scales) over which they form acts to smooth out spatial heterogeneities present in primary emissions.

155 Table S1 summarises the annual averages of emissions (mg m<sup>-2</sup>) from the ECLIPSE<sub>E</sub> inventories, the modelled and measured concentrations (µg m<sup>-3</sup>), and the relative changes in emissions and concentrations between 2010 and 2015 ( $\frac{\text{Difference}}{2010 \text{ data}}$ ), based on the locations of paired model grids with common measurement sites in 2010 and 2015. Entries in Table S1 are shaded according to the magnitude of the relative changes: grey signifies ‘no trend’, where relative differences are within ± 15%; yellow signifies ‘upward trend’, where relative differences are positive by more than 15%; and ‘blue’ signifies ‘downward trend’ where relative differences are negative by more than -15%. It is important to note that the need in this comparison for measurement sites operating in both 2010 and 2015 severely reduces the number of paired comparison data for some measurement networks and therefore lessens the representativeness of comparison results.

165 In some measurement locations and for some species, changes in emissions, modelled and measured concentrations from 2010 to 2015 show consistent upward or downward trends, while for other species in other networks the differences are too small to be considered meaningful given uncertainties inherent in both model and measurements values (and in the

emissions used in the model), and particularly when concentrations are small and hard to measure accurately. A value of  $\pm 15\%$  was chosen as a pragmatic threshold for indicating an upward or downward trend.

Table S1 shows that modelled concentration changes between 2010 and 2015 are highly consistent with the measured trends (and with the trends in emissions) for all three of the precursor gases  $\text{NH}_3$ ,  $\text{SO}_2$  and  $\text{NO}_2$ . For example, the annual average emissions and measured and modelled concentrations of  $\text{SO}_2$  for all networks with  $\text{SO}_2$  data (EANET, UK, EMEP, Canada, and US) all show clear decreasing trends from 2010 to 2015 with relative decreases generally in the range of  $-20\%$  to  $-40\%$ . Similarly, there is consistency between model and measurements (and with emissions) that there is no trend in  $\text{NH}_3$  between 2010 and 2015 for all networks except the China network for which there is again consistency between modelled and measured concentrations that  $\text{NH}_3$  increased between these two years in this region, as do the emissions albeit by a smaller relative amount. (There is also indication of small upward trend in  $\text{NH}_3$  in the US network). For  $\text{NO}_2$ , there is again very good consistency of relative trends between model and measured concentrations of no change in USA, Canada and China, and a decrease in Europe. For the EANET sites the model simulates a somewhat larger decrease in  $\text{NO}_2$  concentrations than ( $-22\%$ ) shown by the measurements ( $-6.4\%$ ) but this comparison is only based on 7 data points.

The responses of secondary species to emission changes from 2010 to 2015 are more complex with clear upward and downward trends as well as no trend appearing in separate networks. For  $\text{SO}_4^{2-}$  concentrations, as for  $\text{SO}_2$  concentrations, both model and measurements are consistent in showing strong decreases between 2010 and 2015 across all the network sites except for EANET for which the model simulates a modest decrease not shown in the measurements.  $\text{NH}_4^+$  concentrations show both clear positive and negative changes in separate networks.  $\text{NH}_4^+$  measurements in China and EANET networks both increase by 18%, whereas modelled  $\text{NH}_4^+$  concentrations both show no obvious trend between 2010 and 2015. For networks in UK and Europe (EMEP/CCC), modelled and measured  $\text{NH}_4^+$  concentrations show similar downward trends all ranging around  $-21\%$ .  $\text{NH}_4^+$  measurements in US and Canada networks decrease by  $-39\%$  and  $-26\%$  respectively, whilst their corresponding modelling data shows smaller decreases. For  $\text{HNO}_3$  and  $\text{NO}_3^-$ , a mixture of upward trend, downward trend, and no trend appears in separate networks and in both model and measurements as well, reflecting a varying response mechanism. In general, however, the 2010 to 2015 relative trends (including no trend) for  $\text{NH}_3$ ,  $\text{NH}_4^+$ ,  $\text{NO}_2$ ,  $\text{HNO}_3$ , and  $\text{NO}_3^-$  are consistent between model and measurements.

Figure S9 shows the modelled global changes in total deposition of reduced N, oxidised N, and oxidised S between 2010 and 2015. In line with precursor emission changes (Figure S6), deposition of reduced N in eastern China and the United States is larger in 2015 than in 2010, whilst deposition over India shows an inverse trend with its emission changes in which 2010 has larger reduced N deposition than 2015 in most grids. For Europe, Africa, and South America regions, the coexistence of both positive and negative differences of reduced N deposition between the two years, makes it difficult to reach a general conclusion of deposition variations in response to emission changes that themselves show both increasing and decreasing trends over these regions from 2010 to 2015. Overall, however, changes in deposition of reduced N between 2010 and 2015 are generally larger than emission changes: only 32% of the relative differences of reduced N deposition are within  $\pm 15\%$  of 2010 annual deposition for that grid (this proportion is 73% for  $\text{NH}_3$  emissions), while 74% of the relative differences are within  $\pm 45\%$  of 2010 annual deposition. The global area-weighted average difference of  $8.24 \text{ mgN m}^{-2}$  corresponds to 8.2% of the global area-weighted average reduced N deposition of 2010. In comparison, changes in oxidised N deposition show both upward and downward trends over eastern China, India, North America, and South America regions, with its global area-weighted average difference ( $-4.15 \text{ mgN m}^{-2}$ ) corresponding to only a  $-3.0\%$  change in the global area-weighted average oxidised N deposition in 2015 compared with 2010. For oxidised S deposition, eastern

China, Europe, and United States all show declining trend from 2010 to 2015 that is consistent with the decreased SO<sub>x</sub> emissions between the two years. The global area-weighted average difference of oxidised S deposition is -13.2 mgS m<sup>-2</sup>, or -12% of its 2010 deposition. As local meteorology plays an important role in deposition process, it is difficult to separately quantify deposition changes that are introduced solely by emission changes between the two years. Additional model experiments with different emission scenarios under the same meteorological conditions are required to gain more insights into the effects of emissions reductions.

In summary, changes in emissions of NH<sub>3</sub> between 2010 and 2015 ECLIPSE<sub>E</sub> inventories are generally small. The global area-weighted average NH<sub>3</sub> emission increases by 4.5% from 2010 to 2015. By contrast, NO<sub>x</sub> and SO<sub>x</sub> emissions show slightly larger variations. The global area-weighted average emissions of NO<sub>x</sub> and SO<sub>x</sub> decrease from 2010 to 2015 by 5.7% and 14% respectively. The trends in modelled NH<sub>3</sub>, NO<sub>2</sub>, and SO<sub>2</sub> annual concentration changes between 2010 and 2015 are entirely consistent with the trends in the emissions supplied to the model, and in the corresponding measurements, given both the realistic uncertainties in emissions and measurements (and the small number of measurement data), and the differential influences of meteorology on concentrations between the two years. Most parts of the world show increased NH<sub>3</sub> concentrations but decreased NO<sub>2</sub> and SO<sub>2</sub> concentrations from 2010 to 2015. The impacts of emission changes on modelled concentrations of secondary pollutants, and modelled total deposition of reduced N, oxidised N, and oxidised S are varying. The comparison of modelled and measured concentration changes based on measurement locations (Table S1) indicates that trends in modelled and measured concentrations for SO<sub>2</sub> and SO<sub>4</sub><sup>2-</sup> in most networks from 2010 to 2015 show clear decreases, while for NH<sub>3</sub>, NH<sub>4</sub><sup>+</sup>, NO<sub>2</sub>, HNO<sub>3</sub>, and NO<sub>3</sub><sup>-</sup> the modelled and measured concentrations reveal a mixture of upward, downward and no trends but are again generally consistent with each other. Overall, the data presented in Figures S6-S9 and in Table S1 of the comparisons of changes in model-simulated concentration and deposition changes between the two years in relation to the changes in measurements (and in the emissions) provide useful additional confirmation that the model is behaving in line with expectations, within realistic levels of measurement uncertainty (given the small number of direct measurement comparisons between the two years that are available).

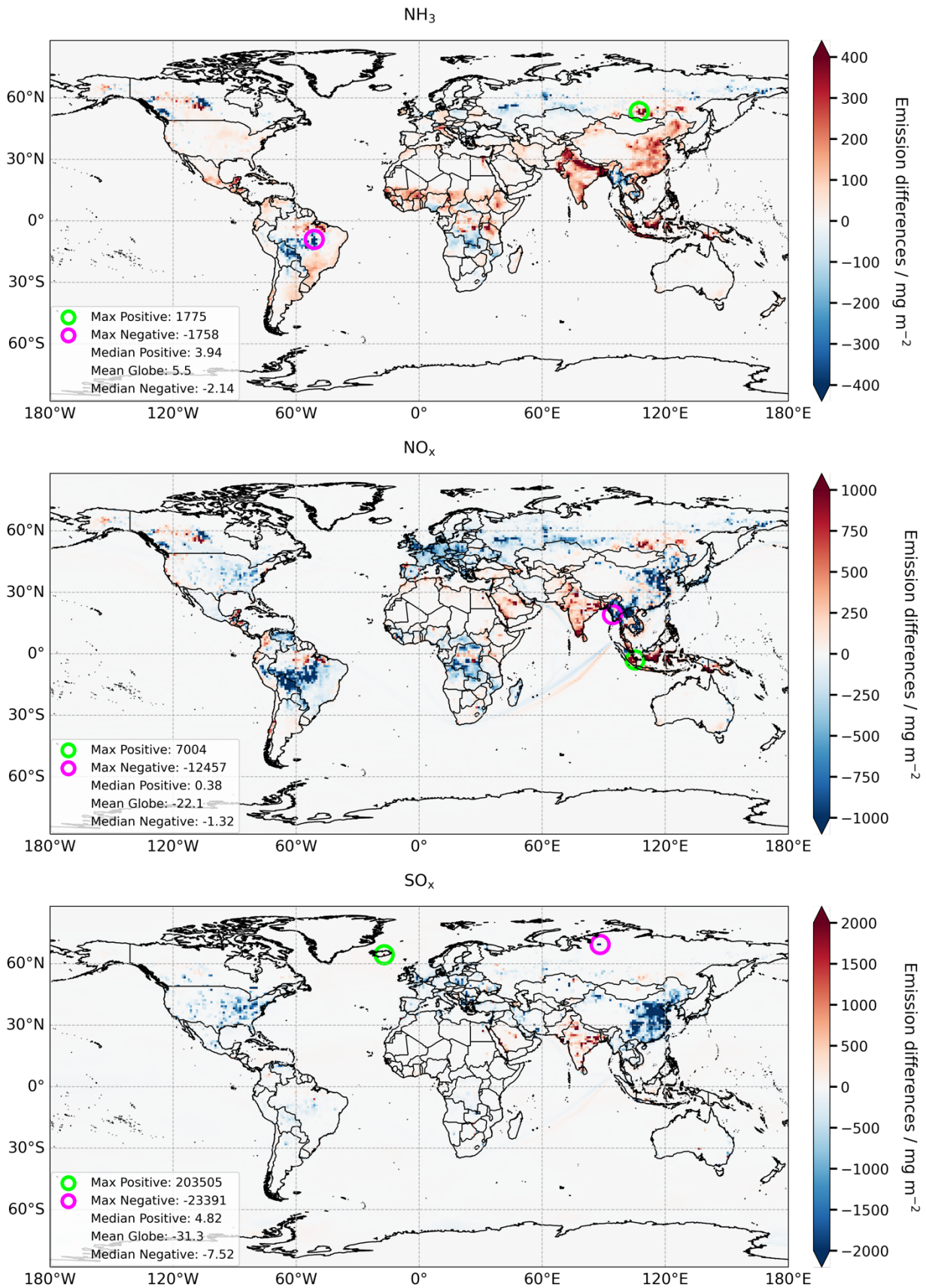
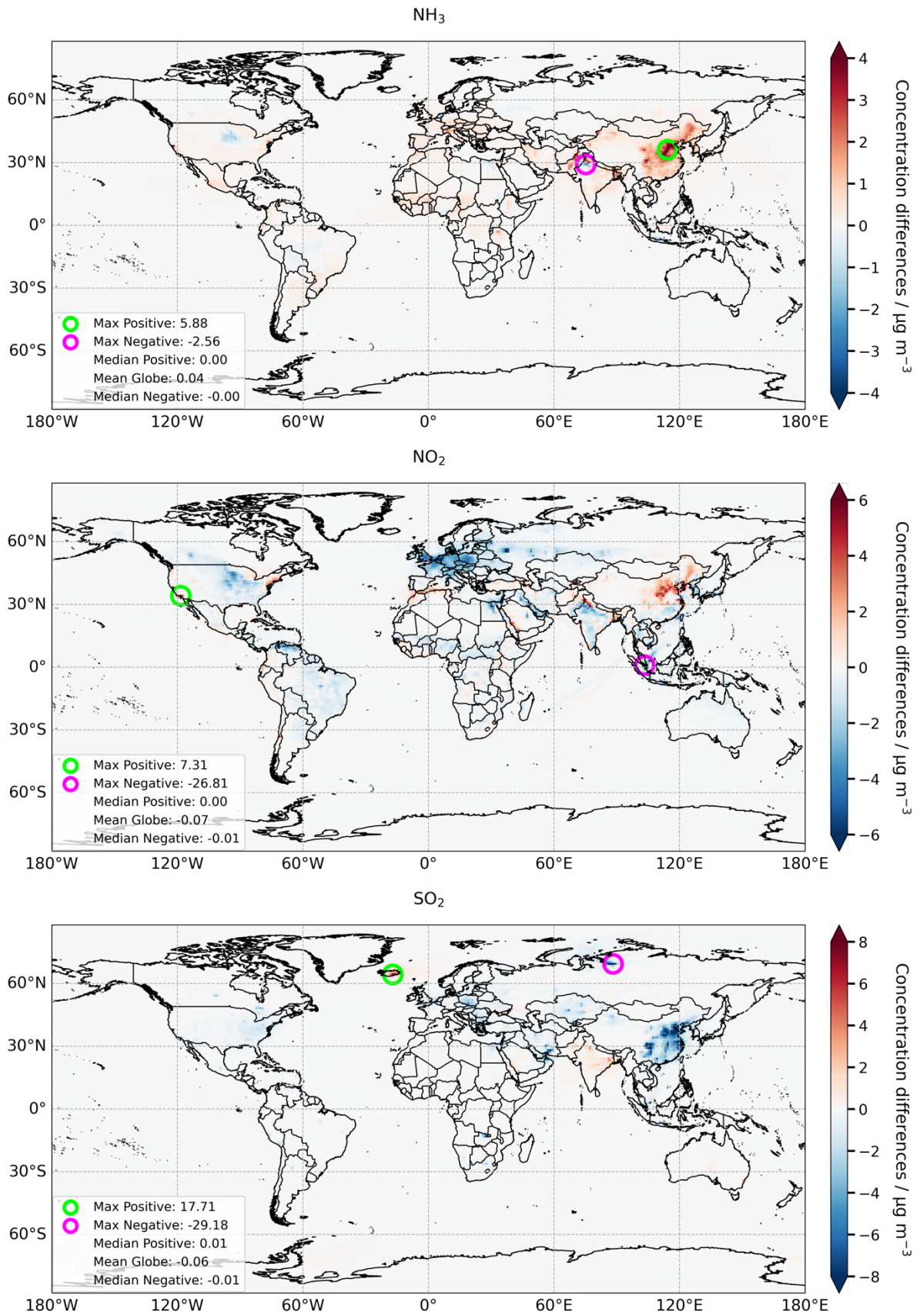
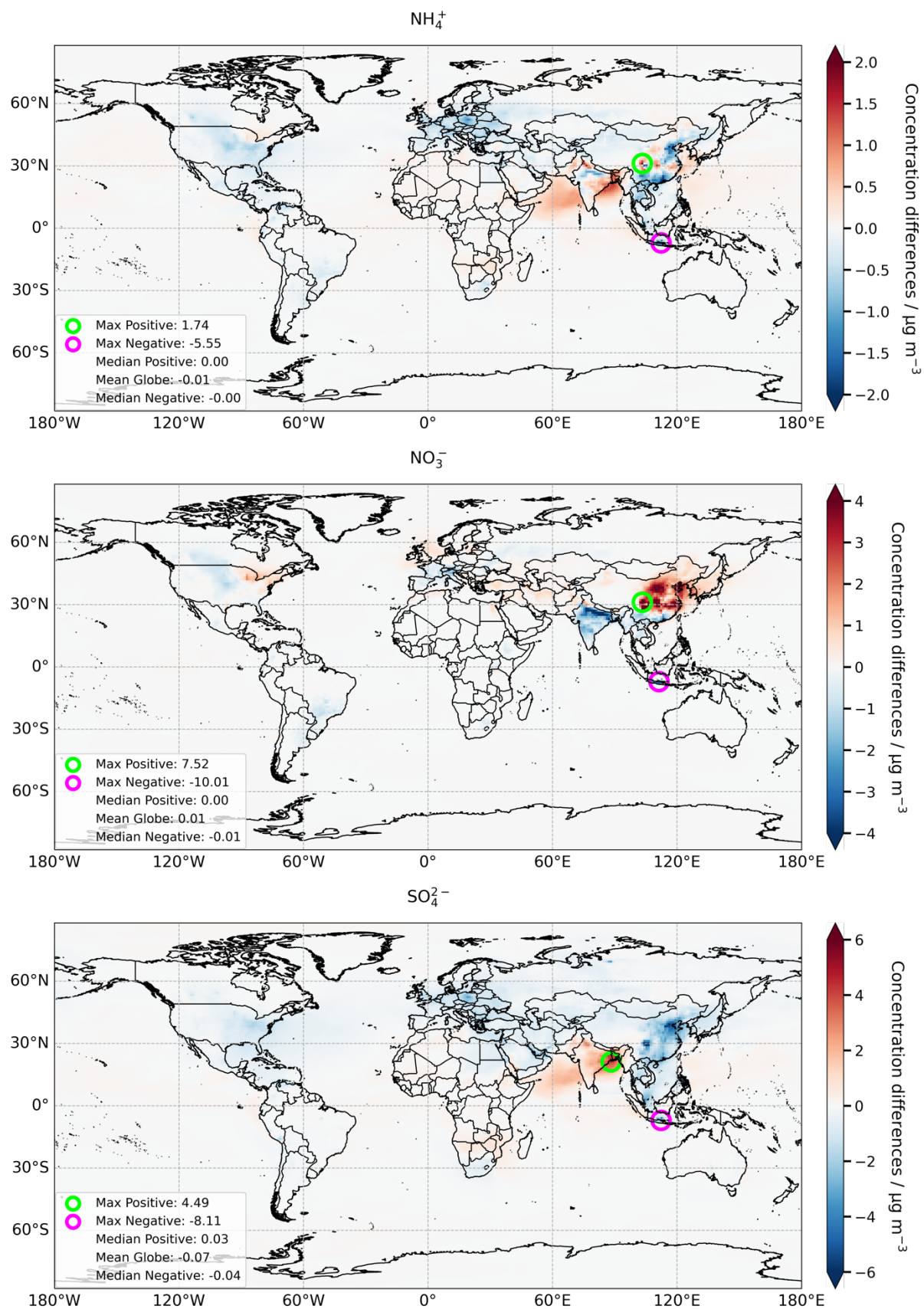


Figure S6. Changes in annual ECLIPSE<sub>E</sub> emissions (in mg m<sup>-2</sup>) between 2010 and 2015 for: top, NH<sub>3</sub>; middle, NO<sub>x</sub>; and bottom, SO<sub>x</sub>. (All expressed as 2015 – 2010.) The inset panel provides the maximum, median and mean values of both positive and negative differences across individual emission grids.

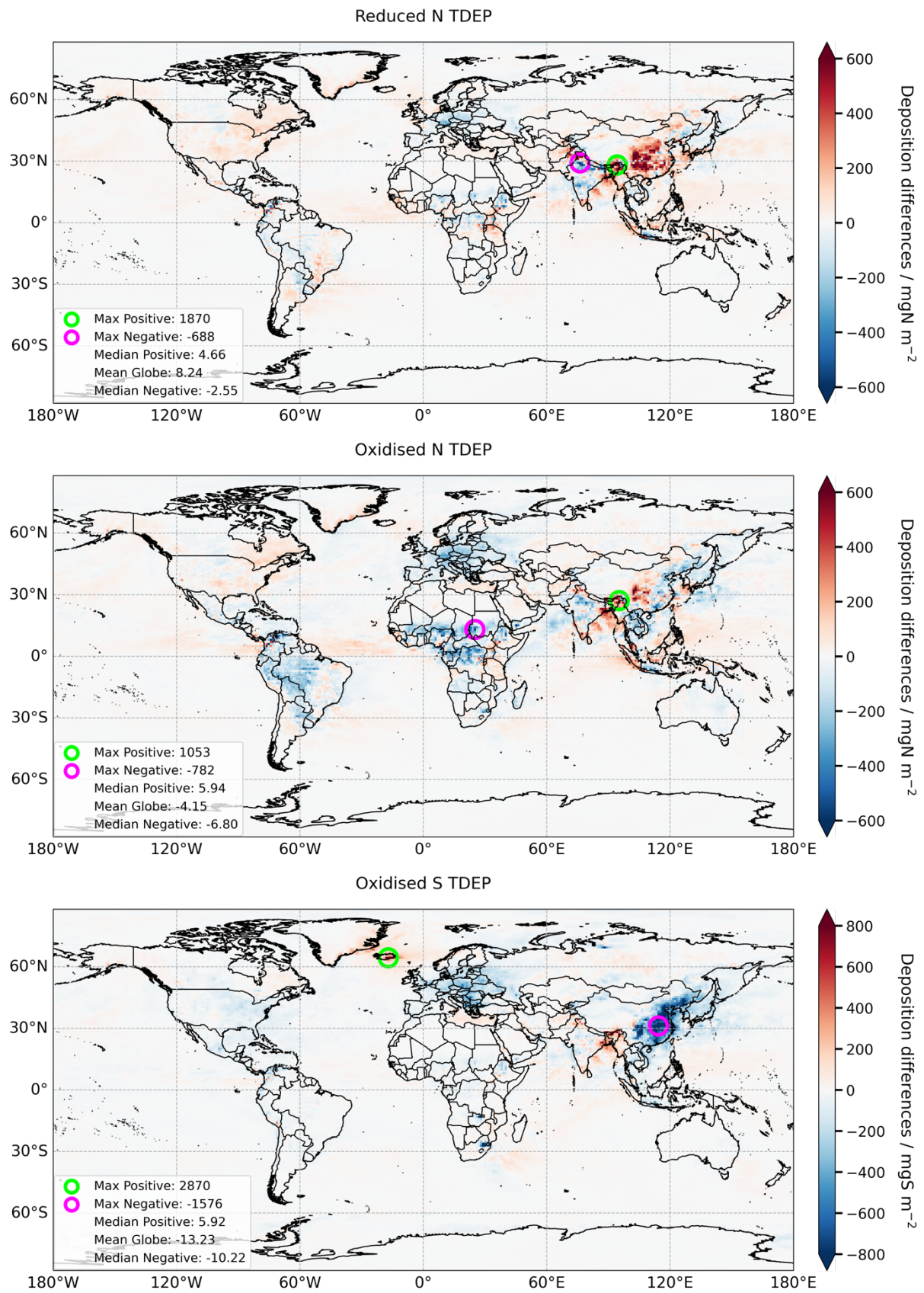


**Figure S7.** Changes in modelled annual average concentrations (in  $\mu\text{g m}^{-3}$ ) between 2010 and 2015, using ECLIPSE<sub>E</sub> emissions inventories for: top,  $\text{NH}_3$ ; middle,  $\text{NO}_2$ ; and bottom,  $\text{SO}_2$ . (All expressed as 2015 – 2010.) The inset panel provides the maximum, median and mean values of both positive and negative differences across individual emission grids.



240

**Figure S8.** Changes in modelled annual average concentrations (in  $\mu\text{g m}^{-3}$ ) between 2010 and 2015, using ECLIPSE<sub>E</sub> emissions inventories for: top,  $\text{NH}_4^+$ ; middle,  $\text{NO}_3^-$ ; and bottom,  $\text{SO}_4^{2-}$ . (All expressed as 2015 – 2010.) The inset panel provides the maximum, median and mean values of both positive and negative differences across individual emission grids.



245

Figure S9. Changes in modelled annual total (wet+dry) deposition between 2010 and 2015, using ECLIPSE<sub>E</sub> emissions inventories for: top, total reduced N deposition (in  $\text{mgN m}^{-2}$ ); middle, total oxidised N deposition (in  $\text{mgN m}^{-2}$ ); and bottom, total oxidised S deposition (in  $\text{mgS m}^{-2}$ ). (All expressed as 2015 – 2010.) The inset panel provides the maximum, median and mean values of both positive and negative differences across individual emission grids.

250 Table S1. Annual averages of emissions ( $\text{mg m}^{-2}$ ) from ECLIPSE<sub>E</sub> inventory and modelled and measured concentrations ( $\mu\text{g m}^{-3}$ ) in 2010 and 2015, based on locations of paired model grids with common measurement sites in both 2010 and 2015. '# of grids' is the number of paired model grids and measurement sites, and 'Model', 'Measu' and 'Emis' are respectively the average modelled concentration, measured concentration and ECLIPSE<sub>E</sub> emissions for those sites/model grids. 'NA' represents that data is not applicable. 'Diff/2010' represents relative differences (2015-2010) in comparison to 2010 data ( $\frac{\text{Difference}}{2010 \text{ data}} \times 100\%$ ). Entries in the table are shaded as follows according to the magnitude of relative trends in 'Model', 'Measu' and 'Emis' between 2010 and 2015: grey means 'no trend', where relative differences are within  $\pm 15\%$ ; yellow means 'upward trend', where relative differences are positive by more than 15%; and 'blue' means 'downward trend', where relative differences are negative by more than -15%.

255

Concentration ( $\mu\text{g m}^{-3}$ )	Emission ( $\text{mg m}^{-2}$ )	# of grids	NH <sub>3</sub>			NO <sub>2</sub>			SO <sub>2</sub>				
			2010	2015	Diff/2010	# of grids	2010	2015	Diff/2010	# of grids	2010	2015	Diff/2010
US	Model		1.57	1.92	22%		9.30	9.61	3.3%		1.84	1.07	-42%
	Measu	6	1.25	1.41	13%	190	15.6	13.9	-11%	173	4.66	2.46	-47%
	Emis		712	732	2.8%		3633	3621	-0.3%		1915	1323	-31%
Canada	Model		1.44	1.50	4.2%		5.67	5.33	-6.0%		1.76	1.31	-26%
	Measu	7	1.37	1.31	-4.4%	65	14.0	12.0	-14%	51	3.30	2.68	-19%
	Emis		656	674	2.7%		2214	2041	-7.8%		1774	1346	-24%
Europe	Model		1.39	1.57	13%		8.19	6.52	-20%		1.30	0.91	-30%
	Measu	21	0.80	0.78	-2.5%	63	1.64	1.39	-15%	60	0.52	0.39	-25%
	Emis		552	551	-0.1%		2150	1853	-14%		718	555	-23%
UK	Model		1.32	1.43	8.3%		NA	NA	NA		1.01	0.71	-30%
	Measu	17	0.90	0.95	5.6%	NA	NA	NA	NA	16	0.62	0.23	-63%
	Emis		693	688	-0.8%		NA	NA	NA		797	539	-32%
EANET	Model		1.60	1.68	5.0%		27.7	25.9	-6.4%		5.78	4.36	-25%
	Measu	20	1.65	1.44	-13%	7	20.0	15.6	-22%	25	6.53	3.74	-43%
	Emis		824	843	2.2%		11794	11523	-2.3%		3225	2547	-21%
China	Model		13.5	15.8	17%		31.0	32.6	5.1%		NA	NA	NA
	Measu	8	8.04	13.0	62%	8	32.5	29.3	-9.9%	NA	NA	NA	NA
	Emis		5947	6189	4.1%		16079	15728	-2.2%		NA	NA	NA

Table S1. Continued

Concentration ( $\mu\text{g m}^{-3}$ )	$\text{NH}_4^+$				$\text{HNO}_3$				$\text{NO}_3^-$				$\text{SO}_4^{2-}$				
	Emission ( $\text{mg m}^{-2}$ )	# of grids	2010	2015	Diff/2010	# of grids	2010	2015	Diff/2010	# of grids	2010	2015	Diff/2010	# of grids	2010	2015	Diff/2010
US	Model		1.33	1.18	-11%		NA	NA	NA		1.14	1.30	14%		1.80	1.29	-28%
	Measu	78	0.90	0.55	-39%	0	NA	NA	NA	203	0.75	0.62	-17%	211	1.39	0.99	-29%
Canada	Model		0.70	0.60	-14%		0.40	0.42	5%		0.72	0.77	6.9%		1.47	1.08	-27%
	Measu	11	0.35	0.26	-26%	7	0.34	0.35	2.9%	11	0.40	0.30	-25%	11	0.96	0.75	-22%
Europe	Model		1.29	1.02	-21%		0.34	0.30	-12%		2.43	2.34	-3.7%		2.12	1.44	-32%
	Measu	31	0.58	0.45	-22%	18	0.13	0.09	-31%	25	0.34	0.32	-5.9%	36	0.56	0.43	-23%
UK	Model		1.34	1.06	-21%		0.34	0.28	-18%		1.91	2.10	9.9%		1.87	1.14	-39%
	Measu	15	0.53	0.42	-21%	17	0.26	0.19	-27%	14	1.19	0.83	-30%	16	0.63	0.43	-32%
EANET	Model		1.24	1.18	-4.8%		1.40	1.31	-6.4%		1.06	1.16	9.4%		3.28	2.79	-15%
	Measu	20	0.57	0.67	18%	18	0.77	0.64	-17%	21	1.11	1.32	19%	21	3.09	3.38	9.4%
China	Model		7.94	7.2	-9.3%		2.20	1.97	-11%		10.9	12.3	13%		NA	NA	NA
	Measu	8	9.05	10.7	18%	8	6.19	5.54	-11%	8	13.0	13.4	3.4%	NA	NA	NA	NA

## Comparison of temporal variation of modelled $\text{NH}_4^+$ concentrations with measurements

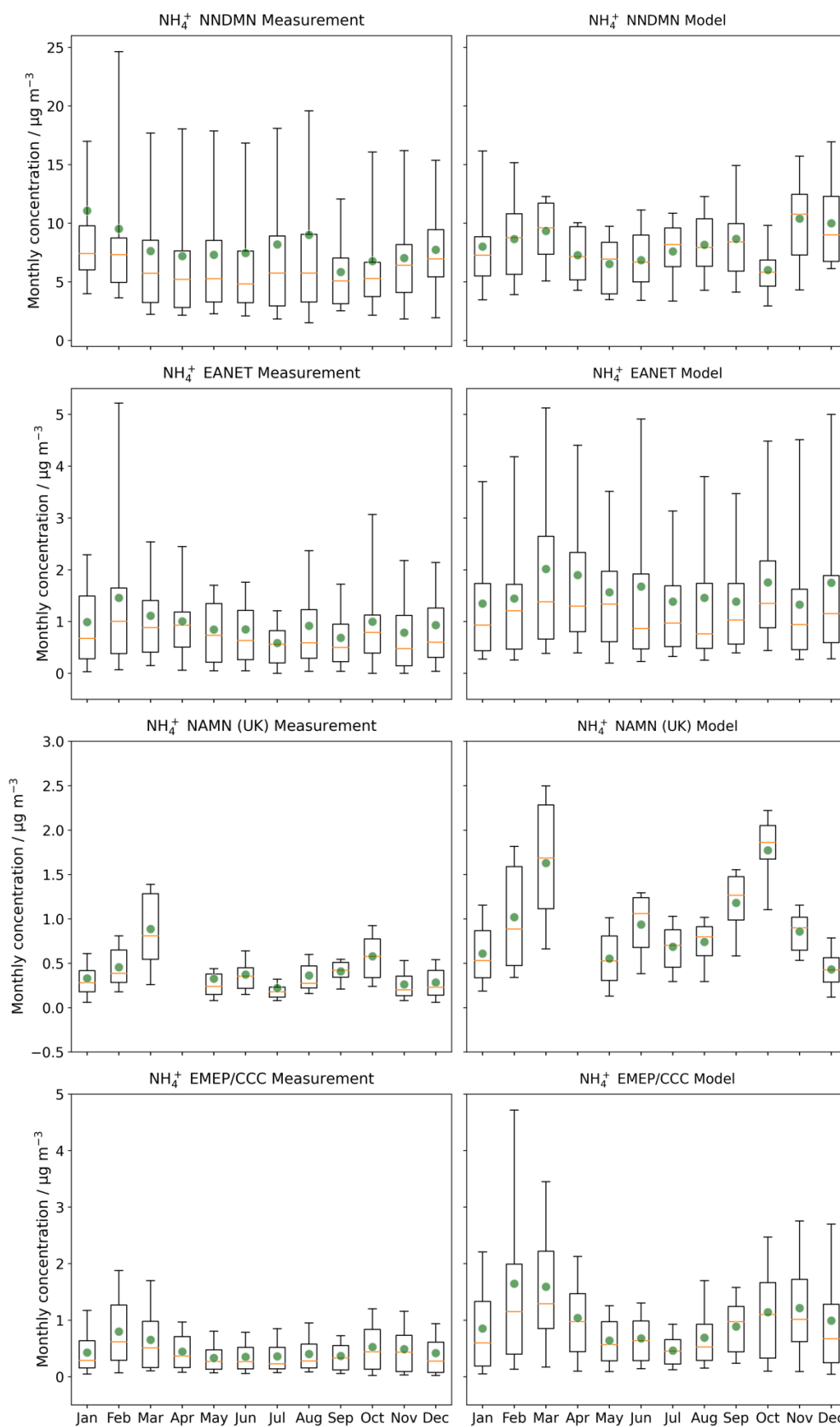
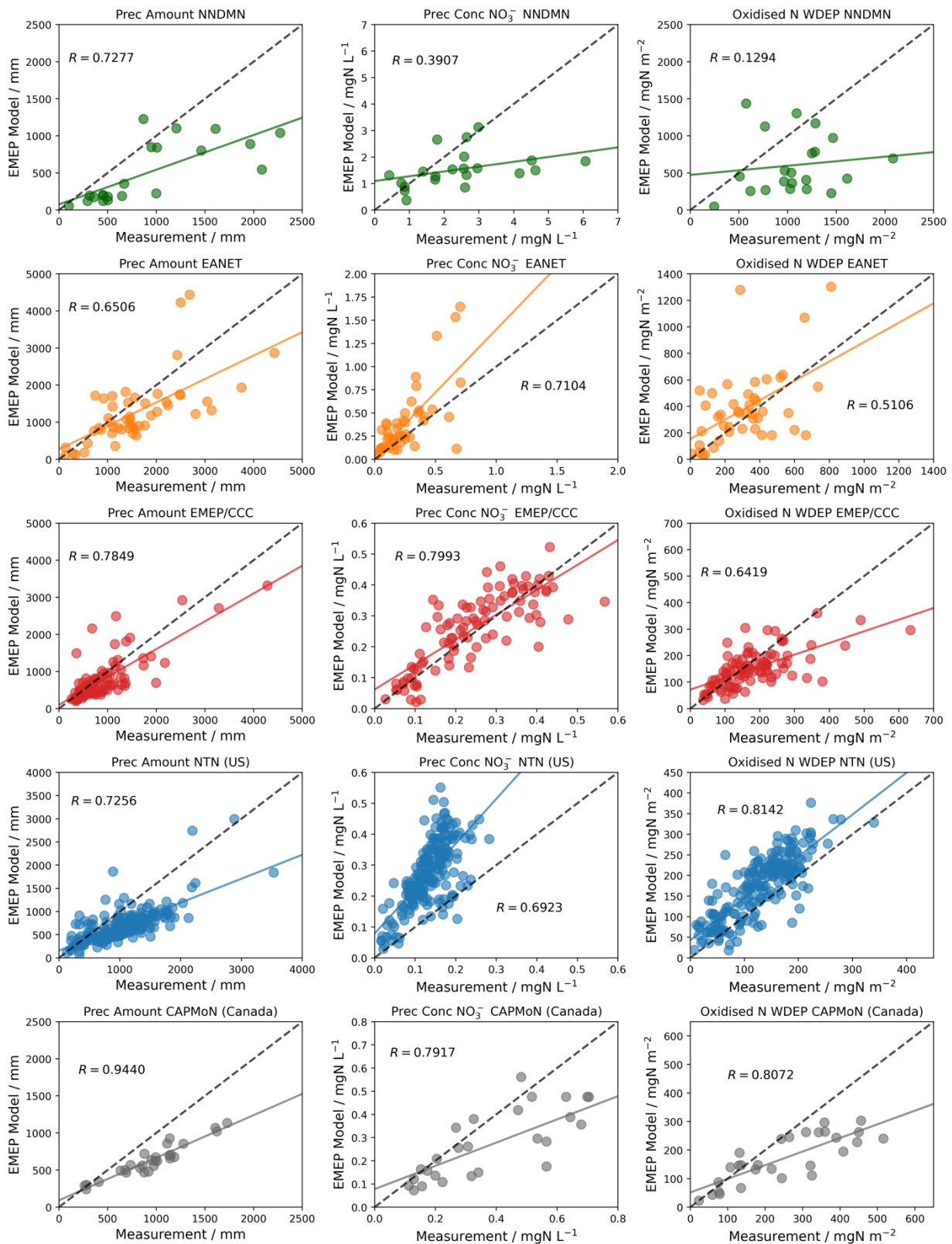


**Figure S10.** Monthly averaged measured (left panels) and modelled (right panels)  $\text{NH}_4^+$  concentrations in 2015 for NNDMN, EANET, AGANet (UK) and EMEP/CCC monitoring networks. The box extends from the lower to upper quartile values of the data, with an orange line at the median and a green point at the mean. The whiskers represent 5% and 95% percentiles.

## Comparison of modelled precipitation and wet deposition with measurements



270

Figure S11. Scatter plots of model-measurement comparisons of 2015 annual wet deposition variables for oxidized N (as  $\text{NO}_3^-$ ) for five measurement networks: NNDMN, EANET, EMEP/CCC, US NTN and Canada CAPMoN. Left panels are annual precipitation. Middle panels are precipitation-weighted annual average  $\text{NO}_3^-$  concentration in precipitation. Right panels are annual total wet deposition of  $\text{NO}_3^-$ . In each plot, the coloured line is the least squares regression and the black dashed line is the 1:1 line.

**Table S2. Summary statistics of model comparison with measurements (referred to here as ‘O’ for observation) for annual precipitation amount (Prec Amount, mm), precipitation-weighted annual mean concentration of NO<sub>3</sub><sup>-</sup> (Prec Conc, mgN L<sup>-1</sup>), and wet deposition of oxidized N (WDEP, mgN m<sup>-2</sup>) for five measurement networks in 2015. *N* is the number of measurement sites. *R* is Pearson’s coefficient. Fac2 fraction is the proportion of data points that are within a factor of 2. Mean\_O and Mean\_M of Prec Conc are annual averages of observation and model respectively. Mean\_O and Mean\_M of Prec Amount and WDEP are annual totals. NMB is normalized mean bias, NME is normalized mean error.**

Networks	Variables	<i>N</i>	<i>R</i>	Fac2 fraction	Mean_O	Mean_M	NMB	NME
China	Prec Amount	21	0.73	0.43	913	502	-0.45	0.49
	Prec Conc	21	0.39	0.67	2.43	1.54	-0.37	0.46
	WDEP	21	0.13	0.38	1068	605	-0.43	0.56
East Asia	Prec Amount	50	0.65	0.82	1585	1270	-0.20	0.39
	Prec Conc	46	0.71	0.59	0.26	0.39	0.52	0.71
	WDEP	44	0.51	0.68	316	384	0.22	0.56
Europe	Prec Amount	101	0.78	0.91	863	749	-0.13	0.31
	Prec Conc	93	0.80	0.92	0.24	0.26	0.06	0.24
	WDEP	93	0.64	0.90	179	151	-0.16	0.32
United States	Prec Amount	206	0.73	0.82	1030	690	-0.33	0.39
	Prec Conc	207	0.69	0.41	0.13	0.27	1.04	1.05
	WDEP	206	0.81	0.87	129	174	0.35	0.41
Canada	Prec Amount	28	0.94	1.00	941	632	-0.33	0.33
	Prec Conc	28	0.82	1.00	0.27	0.29	0.07	0.27
	WDEP	28	0.81	0.79	248	170	-0.32	0.35